

Kinetics of the electrochemical deposition of sulfur from sulfide polluted brines

B.G. ATEYA*, F.M. ALKHARAFI, A.S. ALAZAB and A.M. ABDULLAH

Department of Chemistry, Faculty of Science, University of Kuwait, Kuwait

*(*author for correspondence, e-mail: ateya@kuc01.kuniv.edu.kw)*

Received 5 January 2006; accepted in revised form 17 October 2006

Key words: diffusion, impedance, kinetics, oxidation, passivation, polarization resistance, reaction order, rotating disk electrode, sulfide, sulfur

Abstract

The kinetics of the electrochemical oxidation of sulfide ions in salt water were studied using rotating graphite disc electrodes, polarization techniques, Electrochemical Impedance Spectroscopy (EIS), X-ray Photoelectron Spectroscopy (XPS) and Electron Dispersion Spectroscopy (EDS). Elemental sulfur was shown to be the final product under various temperatures, potentials and times of electrolysis, in amounts that increased with increase in the above variables. The rate of the process is controlled by electron transfer across the interface, while diffusion in the electrolyte has only a modest effect. The apparent reaction orders with respect to the sulfide concentration and pH are 0.60 and 0, respectively. The proposed overall reaction is: $\text{HS}_{(\text{aq})}^- \rightarrow \text{S} + \text{H}^+ + 2\text{e}$, while the rate determining step is: $\text{HS}_{(\text{aq})}^- \rightarrow \text{HS}_{\text{ads}} + \text{e}$. The charge transfer coefficient is $\alpha_a = 0.23$ and the standard rate constant at the equilibrium potential is $k^\circ = 2.2 \times 10^{-7} \text{ cm s}^{-1}$. The degree of coverage of the electrode with sulfur and the polarization resistance of the interface increase, while the current decreases, with the time of electrolysis as more sulfur is deposited on the electrode surface.

1. Introduction

Hydrogen sulfide is a dangerous toxic material [1] which contaminates many industrial water streams and natural water bodies. A prominent example is the massive volumes of geothermal brines that are encountered in the drilling of wells for production of oil and natural gas [2, 3] and for the recovery of geothermal energy. The control of H_2S in oil production is achieved by raising the pH of the brines to about 10, followed by injecting scavengers [3–8], which precipitate H_2S as heavy ion sulfides, oxidize it to elemental sulfur or to other soluble species. Depending on the volume of production, a particular field may require hundreds of tons of scavengers per month, which entails enormous cost and exerts a heavy toll on the environment. Furthermore, the precipitated sulfides and elemental sulfur are dispersed in the drilling fluid to serve as substrates for the sulfate reducing bacteria that regenerate hydrogen sulfide. Hence, the treatment with scavengers provides only a temporary relief from the problems posed by H_2S . The removal of H_2S from these fluids is much more advantageous than its oxidation or precipitation within the brine.

Electrochemical oxidation is one of the approaches that aim to remove hydrogen sulfide from brines [9, 10] and from tannery waste water [11–13]. This approach

can achieve the objective using electrons instead of chemicals and hence can provide the basis of an environmentally sound method of treatment. The anodic oxidation of sulfide ions is also important for the utilization of hydrogen sulfide in fuel cells [14], the electrochemical treatment of white liquor [15], the use of the sulfide/polysulfide redox couples in energy storage [16], the behavior of electrochemical oscillators [17] and for the sensing and electroanalytical determination of sulfide ions [18–21]. The process is complicated by the high reactivity of sulfur and the many oxidation states that it assumes under various conditions [22–25].

The objective of this work is to elucidate the rate processes involved in the anodic oxidation of sulfide ions and to determine the kinetic parameters. Measurements were obtained on rotating disc electrodes, which provide for well defined hydrodynamic conditions at the electrode surface [26].

2. Experimental

Measurements were performed using Gamry (PC4/750 Potentiostat/Galvanostat/ZRA) and an EG&G rotating disc electrode assembly (model 636). The potential was scanned from cathodic towards anodic potentials. A double jacketed polarization cell ($\approx 100 \text{ ml}$) was used

with an Ag/AgCl reference electrode ($E = 0.197$ V (SHE)) and a platinum wire counter electrode. All potentials are reported against this reference electrode. After prolonged use in the sulfide polluted media, several of those platinum wires were broken. Electrochemical impedance (EIS) measurements were performed using an IM5d impedance analyzer (Zahner Elektrik GmbH & Kronach, Germany).

Electrodes were prepared in the form of graphite rods. The cross sectional area of the rod (0.28 cm^2) served as the working electrode. The other surface was coated with Araldite. This eliminates the possibility of reaction on the side surface of the rod. The exposed surface of each electrode was polished successively down to 0.3 and $0.05 \mu\text{m}$ alumina. All measurements were performed in an electrolyte of 3.5% (0.58 M) NaCl containing different concentrations of sodium sulfide. This supporting electrolyte maintains the ionic strength of the electrolyte nearly constant despite the changes in the sulfide concentration (from 0.001 to 0.01 M) and hence minimizes double layer effects on the kinetic parameters. In view of the values of pK_1 and pK_2 of H_2S (7 and ≈ 14 , respectively), the predominant species in this electrolyte is HS^- at pH values from 9 to 12. The test solutions were prepared from deionized water, NaCl (BDH) and Na_2S (BDH). The concentration of sulfide ions was determined iodimetrically. The electrolytes were deaerated by bubbling argon for 25 min before testing. The electrode surfaces were examined using a scanning electron microscope (JSM-6300 JEOL) and an X-ray photoelectron spectrometer, FISONs Instruments, Model ESCA – Lab 200 (VG Instruments). The temperature of the test electrolyte was controlled by flowing hot water around the cell through its double jacketed walls.

3. Results

3.1. Polarization curves

Figure 1 illustrates a potentiodynamic polarization curve obtained in a medium containing 0.58 M NaCl + 0.005 M Na_2S (pH = 11) at a rotation speed of 5000 rpm, a voltage scanning rate $v = 100 \text{ mV s}^{-1}$ and 25°C . The figure shows the results of three runs superimposed on each other to reveal the reproducibility of the measurements. A large number of these curves were measured under different voltage scanning rates, electrode rotation rates, sulfide concentrations and temperatures. As the potential becomes more noble, the anodic current increases. This indicates that the reaction is promoted by the potential, which reveals that the overall rate of the process is affected by charge transfer across the interface. It is shown below that the process is also affected to a smaller extent by diffusion of the sulfide ions in the aqueous phase. The current increases with potential reaching a well defined limiting value, i_L , which remains constant over a broad potential range of hundreds of millivolts. Note the

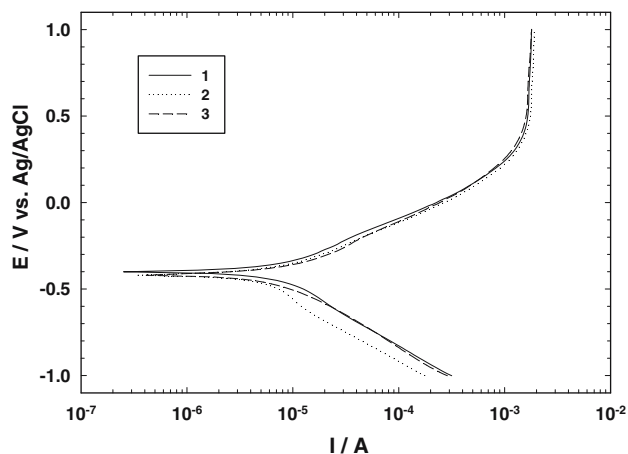


Fig. 1. Current–potential curve for the graphite electrode in the presence of 0.005 M Na_2S at 5000 rpm, a voltage scanning rate of 100 mV s^{-1} and 25°C . The figure shows the results of three different runs under these conditions superimposed on each other.

straight line segment (Tafel region) preceding the limiting current.

3.2. Characterization of the reaction product

Figure 2 illustrates an XPS spectrum measured on an electrode that was polarized in the Tafel region at 0.100 V (Ag/AgCl) for 3 h at 25°C . Some dozens of these XPS spectra were measured under various conditions. A sharp well defined S2p peak appears at 164.1 eV (referred to C1s at 284.6 eV) which is characteristic of the presence of elemental sulfur (S_8) on the electrode surface [27]. This clearly indicates the formation of sulfur (S_8) as a result of the electrochemical reaction. Figure 3 shows an SEM image of an area of the electrode surface after being polarized in the presence of 0.005 M Na_2S for 100 min at 0.450 V (Ag/AgCl) at 25°C . It also shows the EDS spectrum of the region marked with an arrow in the SEM image. A prominent EDS peak appears at about 2.5 keV which is

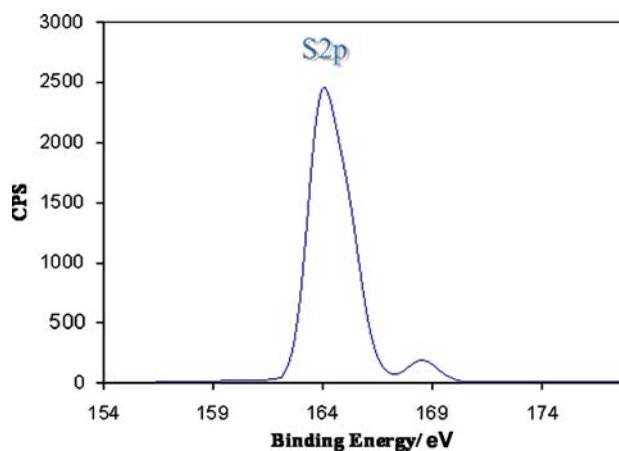


Fig. 2. XPS spectrum of a graphite electrode after being polarized at 0.100 V (Ag/AgCl) for 3 hr in presence of 0.005 M Na_2S at 25°C .

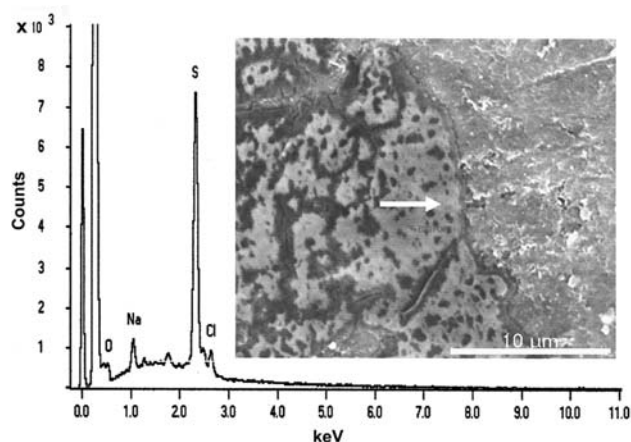
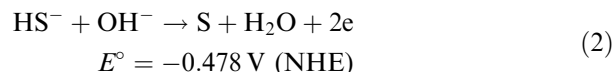
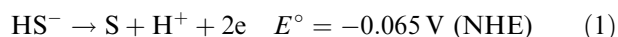


Fig. 3. SEM image of the electrode surface after being polarized for 100 min at 0.450 V (Ag/AgCl) at 25 °C.

characteristic of sulfur. Note also the non-uniform distribution of sulfur on the electrode surface.

Out of the many possible electrochemical reactions of the sulfide ions, the following reactions lead to the formation of elemental sulfur [9, 10, 14]:



The resulting atomic sulfur (S) readily polymerizes to give S_8 which is the more stable form of sulfur under the ambient conditions. The results of thermodynamic calculations suggest that elemental sulfur can also undergo oxidation [22–25] to form soluble oxyanions such as S_2O_3^- or SO_4^- . Furthermore, sulfur might also dissolve in the presence of sulfide ions to form a number of polysulfides such as S_2^{2-} and S_3^{2-} [9, 15, 17].

Similar XPS peaks were found at various potentials on the anodic branch of the curve, from -180 to 450 mV (Ag/AgCl) at temperatures from 25 to 70 °C and times of electrolysis of 15 min to 3 h. EDS spectra (not shown) also reveal that the intensity of the sulfur peak increases with temperature, time and potential. These results indicate that sulfur S_8 is the predominant final product under the above conditions.

The formation and accumulation of sulfur on the electrode surface affects its behavior. Sulfur is virtually an insulator, having an electrical resistivity of $\sim 10^{17}$ ohm cm [28]. Consequently, the locations on the electrode surface that become covered with sulfur will no longer contribute to the reaction. Hence, under a constant potential, one expects the current to decrease progressively with the time as more sulfur is deposited on the electrode surface. This behavior is illustrated by the current transients shown in Figure 4a which reveal continuous decay of the current with time at various potentials, temperatures and rotation rates.

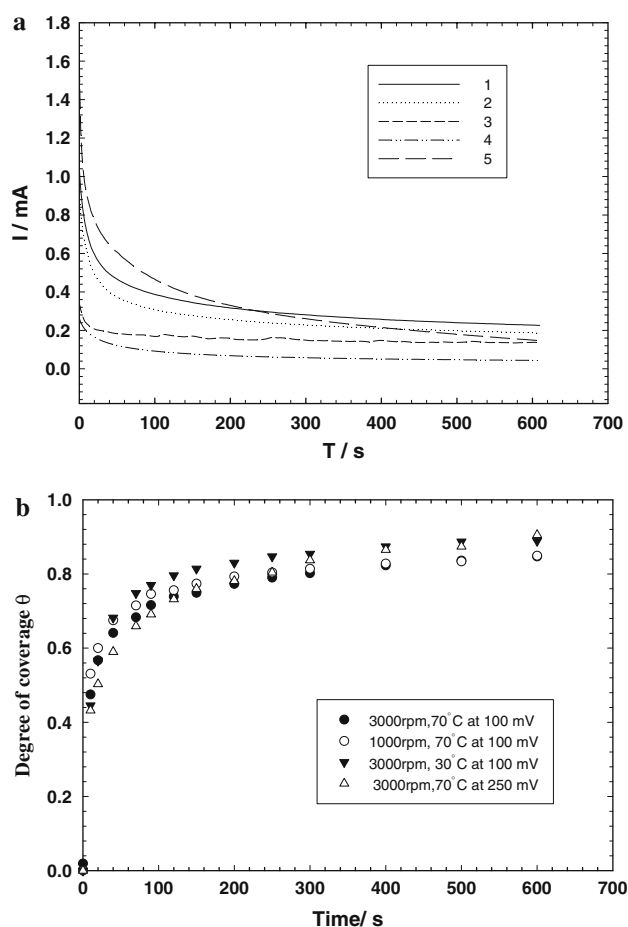


Fig. 4. (a) Current transients supported by a graphite electrode polarized in presence of 0.005 M Na_2S at different rotation rates, temperatures and potentials: (1) 3000 rpm at 70 °C and 0.100 V (Ag/AgCl). (2) 1000 rpm at 70 °C and 0.100 V (Ag/AgCl). (3) 0 rpm at 70 °C and 0.100 V (Ag/AgCl). (4) 3000 rpm at 30 °C and 0.100 V (Ag/AgCl). (5) 3000 rpm at 70 °C and 0.250 V (Ag/AgCl). (b) Time variation of the degree of coverage, $\theta(t)$, of a graphite electrode at different potentials, temperatures and rotation speeds in presence of 0.005 M Na_2S .

The degree of coverage of the surface with elemental sulfur at time t , $\theta(t)$, can be calculated from the measured current transients using the relation:

$$\theta(t) = 1 - i(t)/i(0) \quad (3)$$

where $i(t)$ and $i(0)$ are the currents at times t and 0, respectively. Figure 4b illustrates the variations of $\theta(t)$ with the time of electrolysis at various potentials, temperatures and rotation speeds. Note the initial rapid increase of $\theta(t)$ with time. The value of $\theta(t)$ approaches 0.5 within seconds, at all potentials, times, temperatures and rotation rates. Subsequently $\theta(t)$ increases gradually with time towards a plateau.

3.3. Kinetic parameters

Figure 1 shows a Tafel region which covers a range of anodic currents of about two orders of magnitude. In

this region, the current, i , is related to the potential, E , by the Tafel equation:

$$E = E_{\text{rev}} + (2.3RT/\alpha_a F) \log i - (2.3RT/\alpha_a F) \log i_o \quad (4)$$

where E_{rev} is the equilibrium potential, i_o is the exchange current, α_a is the charge transfer coefficient of the anodic reaction, F , R and T have their usual meaning. The Tafel slope amounts to 260 mV/decade, which corresponds to a transfer coefficient $\alpha_a \approx 0.23$. Such high Tafel slopes might be caused by specific adsorption, diffuse double layer effects, dual barriers, highly asymmetric energy barrier, etc. [29–34].

The exchange current can be obtained by extrapolating the Tafel line to the equilibrium potential of the reaction that supports the current, which is shown below to be Equation 1. Using the Nernst equation, the equilibrium potential of reaction 1 at a concentration of HS^- of 5×10^{-3} M is estimated to be -0.266 (NHE) which is equivalent to -0.463 V (Ag/AgCl). With this information the exchange current is found to be 3.5×10^{-6} A cm^{-2} . The exchange current density is related to the concentration of the electro active species (c) and the standard rate constant of the reaction (k°) at the equilibrium potential by the relation [35, 36]:

$$i_o = zFk^\circ c^{1-\alpha} \quad (5)$$

Using Equation 5 one obtains a value of $k^\circ = 2.2 \times 10^{-7}$ cm s^{-1} at 25 °C. Equation 5 is a special case of the general equation cited in references [35, 36] for a constant concentration of a solid reaction product.

3.3.1. Effect of rotation rate

Figure 5a, b and c illustrate the effects of electrode rotation speed on the current–potential curves at scanning rates of 1, 10 and 100 mV s^{-1} , respectively. The effect of electrode rotation is much more pronounced at the high voltage scanning rate while it has only a modest effect at 10 and 1 mV s^{-1} . This point is addressed below in the light of the amount of sulfur deposited on the electrode surface during a potentiodynamic scan (see 4.4 Coulometric analysis).

For an electrode reaction controlled by diffusion, the limiting diffusion current, i_{LD} , is related to the rotation speed of the electrode and the properties of the system by the Levich equation [26], i.e.

$$i_{\text{LD}} = 0.62zF\omega^{1/2}D^{2/3}\mu^{-1/6}c \quad (6)$$

where zF is the number of coulombs per mole, $\omega = 2\pi f$ is the angular velocity (radian s^{-1}), D is the diffusion coefficient ($\text{cm}^2 \text{s}^{-1}$), μ is the kinematic viscosity ($\text{cm}^2 \text{s}^{-1}$), and c is the concentration of the sulfide ions (mol cm^{-3}). Equation 6 predicts a linear relationship between, i_{LD} and $\omega^{1/2}$. It also predicts the values of limiting currents given by the Levich line in Figure 6 for the values of $z = 2$, $F = 96\,500$ coulomb, $\mu = 0.01$ $\text{cm}^2 \text{s}^{-1}$, $D = 1.37 \times 10^{-5}$ $\text{cm}^2 \text{s}^{-1}$ [37] and $c = 5 \times 10^{-6}$ mol cm^{-3} . The rotating electrode system was

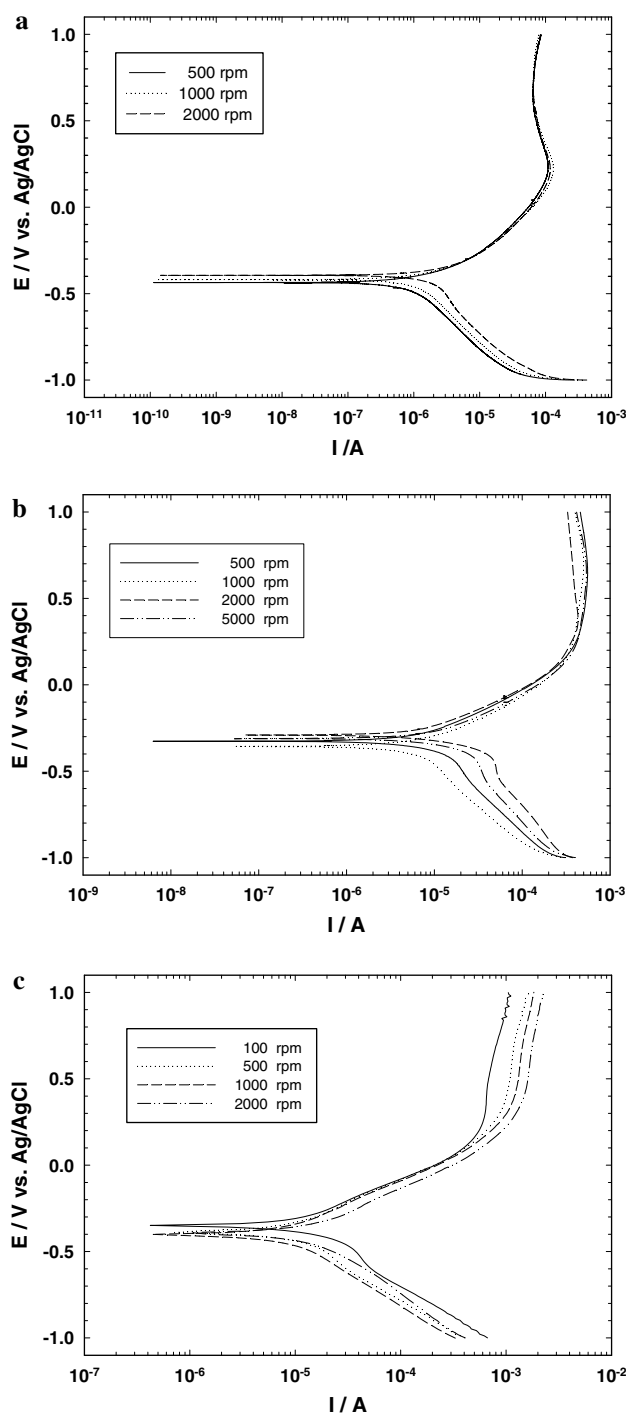


Fig. 5. Effect of electrode rotation rates on the current–potential relations, measured in the presence of 0.005 M Na_2S at 25 °C and at different voltage scanning rates: (a) 1 mV s^{-1} , (b) 10 mV s^{-1} and (c) 100 mV s^{-1} .

tested using the ferri/ferrocyanide couple, where the limiting currents gave perfect fits to the Levich equation.

Figure 6 illustrates the dependence of the experimentally measured limiting current i_{L} on $\omega^{1/2}$ for a sulfide concentration of 0.005 M and different voltage scanning rates at 25 °C. It also shows the variation of i_{LD} with $\omega^{1/2}$, according to Equation 6. The measured limiting current (i_{L}) remains virtually constant independent of $\omega^{1/2}$ at

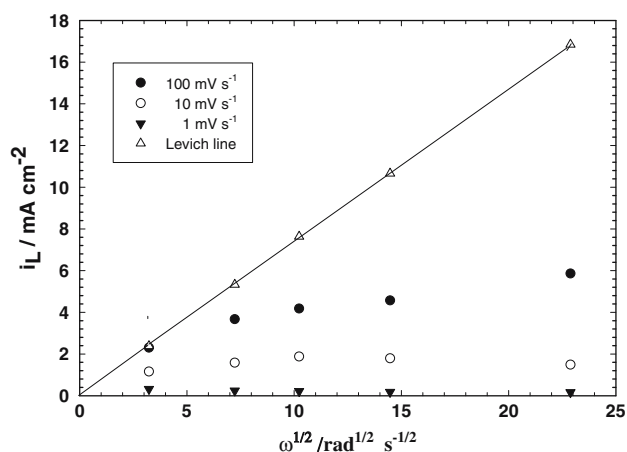


Fig. 6. The relation between i_L and $\omega^{1/2}$ for a graphite electrode in the presence of 0.005 M Na_2S at voltage scanning rates of 1, 10 and 100 mV s^{-1} and 25 °C. The Levich line gives the predictions of Equation 6.

voltage scanning rates of 1 and 10 mV s^{-1} . On the other hand, for the case of 100 mV s^{-1} , i_L increases only modestly with the rotation speed. The measured values of i_L at all rotation speeds and voltage scanning rates are much smaller than those calculated from the Levich equation (i_{LD}) for a diffusion controlled reaction.

The above evidence indicates that the process is predominantly controlled by charge transfer at the interface and only modestly affected by diffusion of the sulfide ions within the electrolyte. The discrepancy of Figure 6 is attributed to the effects of the elemental sulfur which deposits on the surface during the reaction. This point is addressed more quantitatively below.

3.3.2. Effects of concentration and pH

The effect of sulfide concentration on the current–potential relation is illustrated in Figure 7 which shows the results obtained at 100 mV s^{-1} , 5000 rpm and 25 °C. An increase in the sulfide concentration increases the current. Furthermore the current given by the support-

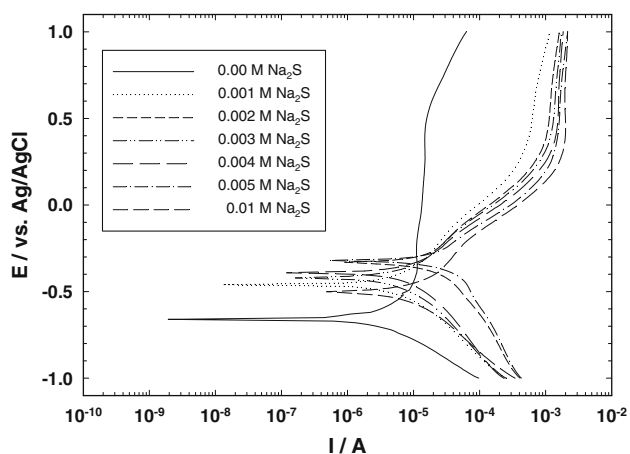


Fig. 7. Current potential curves for the graphite electrode at 25 °C, 5000 rpm and 100 mV s^{-1} in the presence of different concentrations of Na_2S .

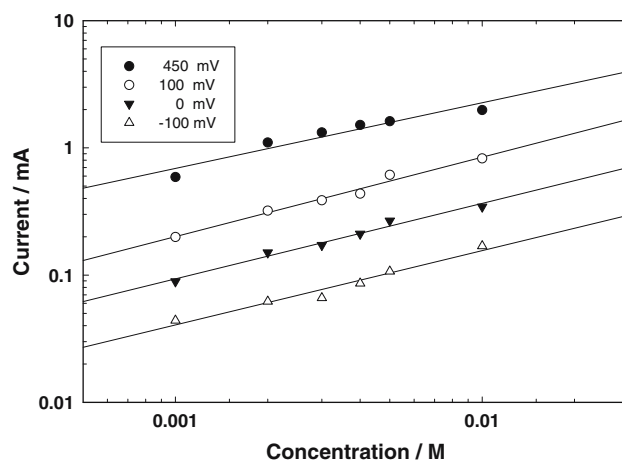


Fig. 8. Logarithmic plot between the current and the concentration of the Na_2S for the graphite electrode at 450, 100, 0 and -100 mV (Ag/AgCl) in a medium of 0.58 M NaCl at 5000 rpm and 25 °C under the same conditions as Figure 7.

ing electrolyte (0.58 M NaCl) is some two orders of magnitude smaller than that provided by the sulfide containing electrolytes. A logarithmic plot of the data is presented in Figure 8 at several values of potential. The results fit satisfactory straight lines at all potentials with nearly equal slopes of 0.60 ± 0.02 , i.e.

$$r(\text{HS}^-) = \left(\frac{\partial \log i}{\partial \log c} \right) \approx 0.60 \quad (7)$$

This value is close to the value of 0.5 measured on platinum [38]. The value of the slope $r(\text{HS}^-)$ is the order of the electrochemical reaction with respect to the sulfide ions in the electrolyte. This is considered an apparent reaction order (r) while the true reaction order (n) is given by the dependence of the current on the degree of coverage of the electrode surface with adsorbed HS^- ions [14].

Similar polarization curves were measured at various pH values (from 9 to 12), 5000 rpm, 100 mV s^{-1} , a concentration of 0.005 M Na_2S and 25 °C (not shown).

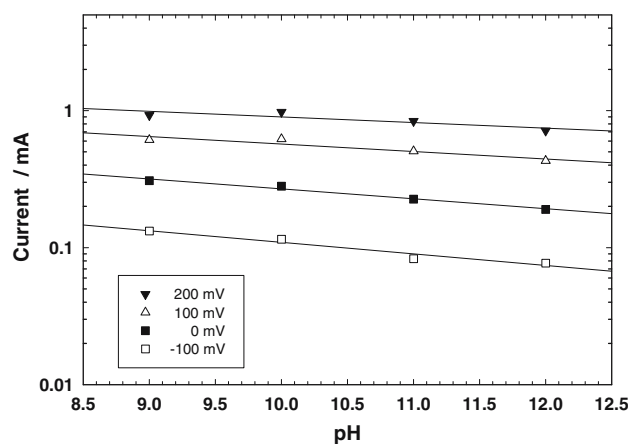


Fig. 9. Logarithmic relation between the current at various potentials and the pH of the electrolyte for the graphite electrode in presence of 0.005 M Na_2S at 5000 rpm, 100 mV s^{-1} and 25 °C.

An increase in the pH had only a negligible effect on the current. Figure 9 shows a logarithmic plot of the current vs. the pH of the medium at several values of potential. The figure shows straight lines at all potentials with negligibly small slopes which are considered to be zero. The slope of the relation is the order of the reaction with respect to the concentration of H^+ (and of OH^-) ions, i.e.

$$r(H^+) = \left(\frac{\partial \log i}{\partial \text{pH}} \right) \approx 0 \quad (8)$$

This indicates that the reaction rate is virtually independent of the pH of electrolyte, in agreement with the results obtained on platinum [38]. Upon comparing this value with the apparent reaction order measured with respect to the concentration of sulfide ions (0.6 ± 0.02), one concludes that the rate of the process is significantly affected by the sulfide concentration and not by the pH of the electrolyte. This indicates that the measured current is supported predominantly by reaction 1, with negligible contributions from reaction 2.

3.3.3. Effect of temperature

Figure 10 displays the polarization curves obtained at 5000 rpm in the presence of 0.005 M Na_2S at 100 mV s^{-1} and different temperatures. The increase in temperature increases the anodic current over a broad range of potentials. For many electrode reactions, the Arrhenius equation has the form [35, 36]:

$$i = A \exp(-\Delta H^\ddagger / RT) \quad (9a)$$

where ΔH^\ddagger is the enthalpy of activation and A is the pre-exponential factor, which includes the entropy of activation, ΔS^\ddagger , i.e. $A = A^- \exp(-\Delta S^\ddagger / RT)$. Consequently, Equation 9a takes the form:

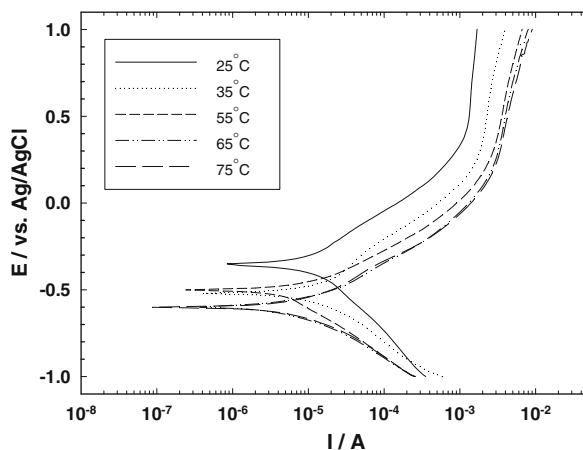


Fig. 10. Current potential curves for the graphite electrode in the presence of 0.005 M Na_2S at 5000 rpm, 100 mV s^{-1} and different temperatures: (a) 25 °C, (b) 35 °C, (c) 55 °C, (d) 65 °C and (e) 75 °C.

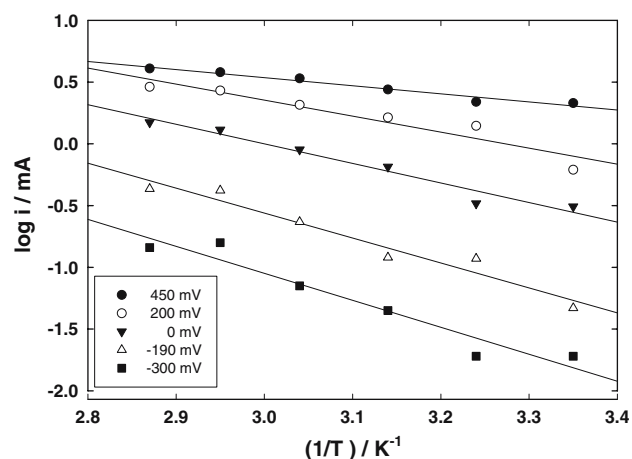


Fig. 11. Arrhenius plots of the results shown in Figure 10 at various potentials.

$$i = A^- \exp(-\Delta G^\ddagger / RT) \quad (9b)$$

where $\Delta G^\ddagger = \Delta H^\ddagger - T\Delta S^\ddagger$ is the free energy of activation of the reaction. Consequently a plot of $\ln i$ vs. $1/T$ would give a straight line from the slope of which ΔG^\ddagger can be calculated. Note that the activation free energy of an electron transfer reaction, ΔG^\ddagger , is considered an apparent value as it depends on the electrode potential [35, 36, 39], i.e.

$$\Delta G^\ddagger = \Delta G_r^\ddagger - \alpha FE \quad (10)$$

where ΔG_r^\ddagger is the activation free energy of the reaction at a reference potential and E is the potential (against this reference) at which the apparent ΔG^\ddagger was measured.

Figure 11 shows Arrhenius plots at 450, 200, 0, -190 and -300 mV (Ag/AgCl). All sets of results give satisfactory straight lines with slopes of -0.656, -1.29, -1.584, -2.019 and -2.39, which yield activation free energies (ΔG^\ddagger) of 5.45, 10.7, 13.2, 16.8 and 19.9 kJ mol^{-1} , respectively. An increase in potential in the anodic direction decreases ΔG^\ddagger , in agreement with the fact that anodic polarization promotes the anodic reaction. The effect of electrode potential on the activation free energy, ΔG^\ddagger , is illustrated in Figure 12. The results fit a straight line in agreement with the predictions of Equation 10. This is another proof that charge transfer across the interface is the rate determin-

Table 1. Variation of the polarization resistance, R_p , with time during anodic oxidation of sulfide ions from an electrolyte containing 0.005 M Na_2S at 25 °C and different potentials, in V (Ag/AgCl)

Time (min)	Polarization resistance (k Ω)	
	0 V	0.250 V
5	6.43	2.39
15	8.66	7.60
30	12.12	12.79
60	16.50	23.89
90	18.79	25.89

ing step. From the slope of the straight line, a value of $\alpha_a = 0.21$ was obtained which agrees with the value of 0.23 calculated from the Tafel slope (see above).

3.4. Electrochemical impedance spectroscopy (EIS)

EIS measurements were performed to obtain the polarization resistance of the interface at various potentials and times of electrolysis. The impedance diagrams were analyzed as shown elsewhere [40]. The results are listed in Table 1. The polarization resistance (R_p) increases with the time of electrolysis, as a result of the accumulation of sulfur on the electrode surface. Furthermore, the rate of increase of R_p with time of electrolysis is greater at the higher than at the lower potential. This is readily explained in the light of the fact that the reaction rate and hence the rate of accumulation of sulfur on the electrode surface are larger at higher potentials. At the beginning of the electrolysis, the polarization resistance is lower at the higher potential. This is consistent with the fact that an increase of anodic potential promotes the reaction and hence decreases the polarization resistance. These results indicate that charge transfer at the interface is the rate determining step, which is being progressively impeded with further deposition of sulfur at increasing potentials and times of electrolysis.

4. Discussion

4.1. Transfer coefficient and activation energy

The Tafel line yields an exchange current density of $i_0 = 3.5 \times 10^{-6} \text{ A cm}^{-2}$ and a transfer coefficient of 0.23 at 25 °C for a solution containing 0.005 M HS^- ion. This corresponds to a standard rate constant of $k^\circ = 2.2 \times 10^{-7} \text{ cm s}^{-1}$ at the equilibrium potential (-0.266 V (NHE)) which reveals that charge transfer is a fairly slow process. The significance of this low transfer coefficient is discussed below. The rate deter-

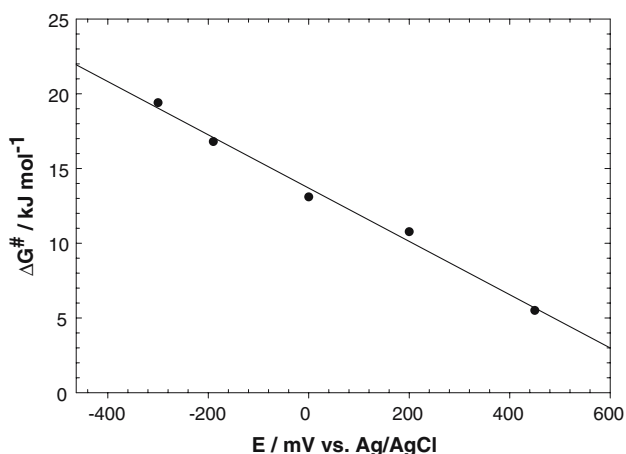


Fig. 12. Effect of electrode potential on the apparent activation energy of the reaction, under the conditions of Figure 10.

mining step is the transfer of one electron from HS^- ion to form an adsorbed intermediate HS_{ads} (c.f. Equation 16). Note that the HS^- is surrounded by an ionic atmosphere that is dispersed during the formation of the activated complex. This process is accompanied by positive entropy of activation which decreases the free energy of activation.

The free energy of activation ΔG^\ddagger decreases linearly with an increase of potential in the anodic direction, see Equation 10 and Figure 12. This indicates that the rate determining step involves charge transfer. From the dependence of ΔG^\ddagger on potential, a transfer coefficient $\alpha_a = 0.21$ was obtained. This value agrees with that ($\alpha_a = 0.23$) obtained independently from the Tafel slope.

4.2. Relevance of oxygen evolution

Similarly low charge transfer coefficients were reported for the oxygen evolution reaction on gold (0.25) and on palladium (0.2) electrodes [41]. The mechanisms proposed for oxygen evolution involve electrochemical adsorption as a rate determining step [14, 32–34, 41–43], e.g.



or



Furthermore, the “apparent” reaction order of oxygen evolution with respect to OH^- ions is 0.5 [42, 43] which is close to the value of (0.6) measured in this work for the oxidation of the HS^- ions. The above findings are relevant as oxygen is the first member of the chalcogenide group in the periodic table, of which sulfur is the second member. The anodic oxidation of HS^- ions to produce sulfur bears some similarity to the oxidation of OH^- to form oxygen. While sulfur is deposited on the electrode surface in the anodic oxidation of sulfide ions, chemisorbed oxygen is an intermediate in the oxygen evolution reaction.

This low value of α has been rationalized on the basis of a dual barrier model for oxygen evolution [14, 33, 34, 41]. The model stipulates that the total potential drop across the interface $\Delta\phi$ is divided among the electrical double layer $\Delta\phi_1$ and the oxide film $\Delta\phi_2$, such that $\Delta\phi = \Delta\phi_1 + \Delta\phi_2$. The overall rate is given by

$$i = k \exp\left(\frac{\beta FE}{RT}\right) \quad (12)$$

where k is a constant and $\beta = \alpha_1 \alpha_2 / (\alpha_1 + \alpha_2)$ while α_1 and α_2 are the charge transfer coefficients at the electrolyte/oxide and oxide/metal interfaces, respectively. Assuming $\alpha_1 = \alpha_2 = 0.5$ and a uniformly covered surface, Equation 12 predicts an effective transfer coefficient of 0.25 which is nearly equal to the measured values.

The dual barrier model cannot be readily extended to the case of sulfur deposition, in spite of the above

mentioned similarities. While an oxide layer on a metal has semi conducting properties (e.g. $\rho \cong 5 \times 10^4$ ohm cm^{-1} at 25 °C for PtO_2) [44] a layer of sulfur (where $\rho \sim 10^{17}$ ohm cm) is virtually an insulator [28]. Furthermore, Figure 3 shows that sulfur deposits non-uniformly. Consequently the perceived role of the deposited sulfur in the oxidation of HS^- ions is different than that of the oxide film in oxygen evolution. The most readily accepted role of the deposited sulfur in the present system is that it gradually passivates the surface as it forms, leaving an ever decreasing fraction of the surface for charge transfer. This conclusion is supported by the SEM images in Figure 3, the progressive increase in the polarization resistance with time and the coulometric calculations given below.

4.3. Reaction order

The dependence of the current on sulfide concentration and pH of the medium revealed reaction orders of 0.60 and 0, respectively, in agreement with earlier results obtained on platinum [38]. This indicates that reaction 1 is the predominant source of the measured current. The reaction order determined by Equation 7 is an apparent value [14, 45] with respect to the bulk concentration of HS^- , c . In reality, however, the reacting ions, HS^- , are adsorbed on the electrode surface at a degree of coverage (θ_{HS^-}). The true reaction order (n) which affects the current concerns (θ_{HS^-}) i.e.

$$n(\theta_{\text{HS}^-}) = \left[\frac{\partial \ln i}{\partial \ln \theta_{\text{HS}^-}} \right] \quad (13)$$

Both reaction orders are related by the following equation [14, 45]

$$R(\text{HS}^-) = n(\text{HS}^-) \frac{\partial \ln(\theta_{\text{HS}^-})}{\partial \ln c} \quad (14a)$$

The expression of the derivative $\partial \ln(\theta_{\text{HS}^-})/\partial \ln c$ depends on the particular isotherm of adsorption of HS^- ions on the surface, which relates (θ_{HS^-}) and c . Its value is usually less than one, hence the true reaction order (n) is always greater than the apparent value (r). For the case of the Langmuir isotherm, the derivative $\partial \ln \theta_{\text{HS}^-} / \partial \ln c = 1 - \theta_{\text{HS}^-}$ and the above relation takes the form [14, 45]:

$$r = n(1 - \theta_{\text{HS}^-}) \quad (14b)$$

Table 2. Variation of the charge passed (σ / $\mu\text{C cm}^{-2}$) and the amount of sulfur deposited (Δm / mol cm^{-2}) at various potentials during the anodic sweep in Figure 1

E (V)	q ($\mu\text{C cm}^{-2}$)	Δm (mol cm^{-2})
-0.200	66.8	3.46×10^{-10}
0.000	536	2.78×10^{-9}
0.200	2995	1.56×10^{-8}
0.400	8964	4.65×10^{-8}
0.600	18300	9.48×10^{-8}
0.800	28607	1.48×10^{-7}
1.000	40642	2.11×10^{-7}

Other isotherms give more complex relations. At the limit of $\theta_{\text{HS}^-} \rightarrow 0$, $r = n$, i.e. the true and apparent reaction orders become equal. On the other hand, as $\theta_{\text{HS}^-} \rightarrow 1$, the apparent reaction order approaches zero [46]. This indicates that the true reaction order for HS^- is actually greater than 0.6. The present system is further complicated by the deposition of sulfur on the electrode surface such that the uncovered fraction of the electrode surface is actually $(1 - \theta_{\text{S}} - \theta_{\text{HS}})$ where θ_{S} is the degree of coverage of the surface with sulfur.

4.4. Coulometric analysis

The amount of sulfur deposited on the electrode can be estimated from a calculation of the charge passed. From computation of the area under the anodic curve in Figure 1 and the application of Faraday's law to Equation 1, one can estimate the amount of sulfur deposited on the electrode up to a certain point during a potentiodynamic scan. Table 2 summarizes the results. They reveal that a change of potential in the noble direction increases the amount of sulfur deposited on the electrode. Hence, a greater fraction of the surface area of the electrode is covered with sulfur and a smaller fraction is available to support the electrochemical oxidation of the sulfide ions.

The fact that the rotation speed of the electrode has no significant effect on the rate of the process at low voltage scanning rates is attributed to the electrodeposited sulfur. This point is illustrated by comparing the amounts of sulfur deposited on the electrode surface during the potentiodynamic scans in Figure 5(a, b and c). To illustrate the salient point and to facilitate the comparison, we calculated the time elapsed and the amounts of charge passed during a segment (from 10 to 100 μA) in Figure 5(a, b and c) were calculated. Using Faraday's law and Equation 1, these charges were converted to moles of sulfur per cm^2 . The results are summarized in Table 3. An increase of the voltage scanning rate from 1 to 10 mV s^{-1} results in a decrease of about 20-fold in the amount of charge passed and hence in the amount of sulfur deposited on the electrode surface. Furthermore, an increase of voltage scanning rate from 10 to 100 mV s^{-1} produces an additional 10-fold decrease in the amount of charge passed and hence in the amount of sulfur deposited on the electrode surface. This also explains the disappearance of a meaningful Tafel region in Figure 5(a and b) (at low voltage scanning rates where excessive amounts of sulfur

Table 3. Effect of voltage scanning rate (v) on the time (t (s)), amount of charge passed (q / $\mu\text{C cm}^{-2}$) and amount of sulfur deposited, (Δm / mol cm^{-2}), during potentiodynamic scans from 10 to 100 μA (see Figure 5(a, b and c))

v (mV s^{-1})	t (s)	q / $\mu\text{C cm}^{-2}$	Δm / (mol cm^{-2})
100	2.5	364.3	1.89×10^{-9}
10	22	3421	1.77×10^{-8}
1	418	70642	3.66×10^{-7}

are deposited) and its appearance at a voltage scanning rate of 100 mV s^{-1} (Figure 5(c)). For this reason, measurements were performed at high voltage scanning rates to reveal the electrochemical behavior of the system before substantial accumulation of sulfur blocks the electrode surface.

In view of the above results and reasoning, one envisages the picture of the electrode surface during a potentiodynamic scan as composed of an increasing fraction that is covered with islands of sulfur and a continuously decreasing fraction of uncovered area on which the HS^- ions are being oxidized.

4.5. Proposed mechanism

In view of the above results a plausible mechanism for reaction 1 is visualized. The first step is the adsorption of HS^- ions to form HS_{ad}^- on the electrode surface, at the active locations which are not covered by sulfur, i.e.:



The tendency for sulfide ions to undergo specific adsorption is well documented [31, 47].

The slow step involves discharge of the HS_{ads}^- with the transfer of one electron, to form an adsorbed intermediate HS_{ads} i.e.



The adsorbed intermediate HS_{ads} might be involved in subsequent electrochemical or chemical reactions, i.e.



Equation 19 is a chemical reaction, the rate of which is not strongly dependent on potential, while the rates of reactions 18 and 19 depend on the pH of the medium. This is contrary to the experimental findings. Furthermore, reaction 17 is not consistent with the measured reaction orders. This leaves Equation 16 as the rate determining step.

As the reaction proceeds, the electrode surface becomes covered with sulfur to a degree that increases with time and with potential. This sulfur is shown to be the predominant final product under the above conditions. As the degree of coverage of the surface with sulfur, θ_s , increases, at a certain potential, temperature and rotation rate, the current supported by the uncovered fraction of the surface ($1 - \theta_s$) progressively decreases. A gradual increase in potential (as in Figures 1, 7, 9 and 10) supports a progressively higher current which further increases θ_s with time. As $\theta_s \rightarrow 1$, further increase in potential is required to produce a

constant measured current from a gradually decreasing unblocked fraction ($1 - \theta_s$) of the electrode surface. Hence, we observe a limiting current. Therefore it is concluded that the measured limiting currents are not caused by slow diffusion in the electrolyte but rather by slow charge transfer across the interface as a result of the progressive blocking effect of the elemental sulfur produced by the reaction.

5. Conclusions

The anodic oxidation of HS^- ions on graphite produces elemental sulfur, which has a strong effect on the kinetics of the process. The process is controlled by charge transfer across the interface and only modestly by diffusion of the sulfide ions in the electrolyte. This is borne out by the strong dependence of the current and activation energy on potential and the lack of a significant effect of electrode rotation rate on the measured limiting current. As more sulfur is deposited, the electrode surface is progressively passivated and diffusional effects become less pronounced. This is true even at fairly high voltage scanning rates before accumulation of substantial amounts of sulfur on the surface. Elemental sulfur was identified using XPS and seen on the electrode surface using SEM. The process offers a clean electrochemical approach to the removal of hydrogen sulfide from polluted brines. Successful use of the process requires a solution to the problem of electrode passivation.

Acknowledgements

The authors gratefully acknowledge the support of this work by the Research Administration of Kuwait University, under Grant Numbers SC04/99 and SC04/04 and the use of the ESCA VG Esca lab 200 under General Facility project GS01/01. They also acknowledge the help of the unit of Electron Microscopy for the SEM and EDS measurements.

References

1. U.S. Environmental Protection Agency, *Extremely Hazardous Substance: Superfund Chemical Profiles*, CAS Registry Number 7783-06-4, Vol. 1, (Noys Data Corporation, New Jersey, 1988).
2. H.C.H. Darely and G.R. Gray, *Composition and Properties of Drilling and Completion Fluids*, 5th ed., (Gulf Publishing Company, Houston, 1988), pp. 477.
3. L. Garverick (Ed), *Corrosion in the Petrochemical Industry* (ASM International, Metals Park, Ohio, 1994) p. 259.
4. R.L. Garrett, R.K. Clark, L.L. Carney and C.K. Grantham, *Chemical Scavengers for Sulfides in Water-Based Drilling Fluids*, *SPE Reprint Series* **44** (1997) 170.
5. A.K. Singh, B.S. Kohil and R.P. Wendt, *World Oil* **209** (1989) 99; *ibid.*, **209** (1989) 77.
6. A.Y. Al-Humaidan and H.A. Nasr-El-Din, Optimization of Hydrogen Sulfide Scavengers used during Well Stimulation, *in*

- 'Proceedings of the (1999), SPE International Symposium on Oilfield Chemistry' (1999).
7. P.Chr. Schorling, M. Brauchle, *Application of Hydrogen Sulfide Scavenger in the Oil and Gas Field, Erdoel Ergas Kohle/EKEP* **117** (2001) 78.
 8. P. Scott, *Oil & Gas J.* **92** (1994) 72.
 9. Z. Mao, A. Anani, R.E. White, S. Srinivasan and A.J. Appleby, *Electrochem. Soc.* **138** (1991) 1299.
 10. B.G. Ateya and F.M. Al-Kharafi, *Electrochem. Commun.* **4** (2002) 231.
 11. G. Rajalo and T. Petrovskaya, *Environ. Technol.* **17** (1996) 605.
 12. N.N. Rao, K.M. Somasekhar, S.N. Kaul and L. Szpyrkowicz, *J. Chem. Technol. Biotechnol.* **76** (2001) 1124.
 13. L. Szpyrkowicz, S.N. Kaul and R.N. Neti, *J. Appl. Electrochem.* **35** (2005) 381.
 14. J.O.M. Bockris and Shahid Khan, *Surface Electrochemistry: A Molecular Level Approach* (Plenum Press, London, 1993) p. 951, p. 585.
 15. M. Behm and D. Simonsson, *J. Appl. Electrochem.* **27** (1997) 507.
 16. P.M. Lessner, F.R. McLarnon, J. Winnick and E.J. Cairns, *J. Appl. Electrochem.* **22** (1992) 927.
 17. A. Chen and B. Miller, *J. Phys. Chem.* **108B** (2004) 2245.
 18. A.B. Florou, M.I. Prodromidis, M.I. Karayannis and S.M. Tzouwara-Karayanni, *Talanta* **52** (2000) 465.
 19. H. Ding, V. Erokhin, M.K. Ram, P. Sergio and C. Nicolini, *Mater. Sci. Eng. C: Biomim. Supermole. Syst.* **11** (2000) 121.
 20. W. Yourong, Y. Heqing and W. E' feng, *J. Electroanal. Chem.* **497** (2000) 163.
 21. N.S. Lawrence, J. Davis and R.G. Compton, *Talanta* **52** (2000) 771.
 22. A.J. Bard, R. Parsons and J. Jordan (Eds), *Standard Potentials in Aqueous Solutions* (Marcel Dekker Inc., New York, 1985), p. 94.
 23. S.I. Zhdanow. in A.J. Bard (Ed), *Encyclopedia of the Electrochemistry of the Elements 6*, (Marcel Dekker, New York, 1982).
 24. G. Valensi, J. van Muylder and M. Pourbaix. in M. Pourbaix (Ed), *Atlas of Electrochemical Equilibria in Aqueous Media*, (NACE, Texas, 1974), pp. 545.
 25. E. Protopopoff and P. Marcus, *Corros. Sci.* **45** (2003) 1191.
 26. V.G. Levich, *Physicochemical Hydrodynamics* (Prentice-Hall Inc., Englewood Cliffs, New Jersey, 1962) p. 69 and p. 78.
 27. A.R. Gerson and T. Bredow, *Surf. Interface Anal.* **29** (2000) 145.
 28. J.A. Dean (Ed), *Lange's Handbook of Chemistry*, 15th ed., (McGraw- Hill, New York, 1999), p. 4.2.
 29. L.M. De Silva, L.A. De Faria and J.F.C. Boodts, *Electrochim. Acta* **48** (2003) 699.
 30. V.M. Tsioskii, L.I. Krishtalik and L.B. Kriksunov, *Electrochim. Acta* **33** (1988) 623.
 31. M.L. Foresti, M. Innocenti, F. Forni and R. Guidelli, *Langmuir* **14** (1998) 7008.
 32. L.M. Da Silva, D.V. Franco, L.A. De Faria and J.F.C. Boodts, *Electrochim. Acta* **49** (2004) 3977.
 33. R.E. Meyer, *J. Electrochem. Soc.* **107** (1960) 847.
 34. J.J. MacDonald and B.E. Conway, *Proc. Roy. Soc.* **269** (1962) 419.
 35. A.J. Bard and L.R. Faulkner, *Electrochemical Methods: Fundamentals and Applications*, 2nd ed., (Wiley, New York, 2001), pp. 95.
 36. C.M.A. Brett and A.M.O. Brett, *Electrochemistry, Principles, Methods and Applications* (Oxford University Press, Oxford, 1993) p. 73 and p. 76.
 37. R. Mills and V.M.M. Lobo, *Self Diffusion in Electrolyte Solutions* (Elsevier Science Publisher B.V., Amsterdam, 1989), pp. 318.
 38. S. Kapusta, A. Viebeck, S.M. Wilhem and N. Hackerman, *J. Electroanal. Chem.* **153** (1983) 157.
 39. K.J. Vetter, *Electrochemical Kinetics: Theoretical and Experimental Aspects* (Academic Press, New York, 1967), pp. 115.
 40. F. Mansfeld, H. Shih, H. Green and C.H. Tsai, in J.R. Scully, D.C. Silverman and M.W. Kendig (Eds), *Analysis of EIS Data for Common Corrosion Processes. Electrochemical Impedance: Analysis and Interpretation* (ASTM STP 1188, American Society for Testing and Materials, Philadelphia, 1993), p. 37.
 41. J.P. Hoare. in A.J. Bard (Ed), *Encyclopedia of the Electrochemistry of the Elements 2*, (Marcel Dekker, New York, 1974), pp. 282.
 42. V.I. Birss and A. Damjanovic, *J. Electrochem. Soc.* **130** (1983) 1694.
 43. J.W. Schultze and K.J. Vetter, *Electrochim. Acta* **18** (1973) 889.
 44. L. Maya, E.W. Hagaman, R.K. Williams, X.-D. Wang, G.D. Del Cul and J.N. Fiedor, *J. Phys. Chem. B* **102** (1998) 1951.
 45. E.J. Rudd and B.E. Conway. in B.E. Conway, J.O'M. Bockris and E. Yeager (Eds), *Comprehensive Treatise of Electrochemistry 7*, (Plenum Press, New York, 1980), pp. 641.
 46. H. Wendt and G. Kreysa, *Electrochemical Engineering: Science and Technology in Chemical and Other Industries* (Springer, Berlin, 1999), pp. 51.
 47. A. Bagreev and T.J. Bandosz, *J. Phys. Chem. B* **104** (2000) 8841.